Supporting Information

Electrocatalytic Oxygen Evolution Activity of Surfactant-free Cobalt- and Manganese-based Spinel Oxide Nanoparticles in Acid

Jiajie Liu[a*]; Yvpei Li[a]; Jingguo Du[b]; Rongrong Cao[c]; Zhihao Zeng[d]; Chuanqing Huang[a]; Chao Wang[a, e*]

a College of Chemistry and Chemical Engineering, Shaanxi Key Laboratory of Chemical Additives for Industry, Ministry of Education, Shaanxi University of Science& Technology, Xi'an 710021, China;

b Hebei Province Mining Area Ecology Restoration Industry Technology Research Institute, North China University of Science and Technology, Tangshan 063210, China;

c Oil and Gas Technology Research Institute, Changqing Oilfield Branch Company, CNPC, Xi'an, 710018, China

d Engineering Technology Research Institute of Petrochina Southwest Oil & Gasfield Company, Chengdu, 610017, China.

e Shaanxi Collaborative Innovation Center of Industrial Auxiliary Chemistry & Technology, The Youth Innovation Team of Shaanxi Universities, Shaanxi University of Science and Technology, Xi'an, Shaanxi 710021, P. R. China

*Corresponding author.
E-mail address: liujiajie@sust.edu.cn
                cwang@sust.edu.cn

1. Experimental

2. Instrumentation

3. X-ray photoelectron spectroscopy

4. X-ray diffraction

5. EDS and ICP-AES

6. Electrochemistry

7. Activity comparison

8. TEM

9. References

1. Experimental

Chemicals

Cobalt(II) tetrahydrate (Co(ac)$_2$•4H$_2$O; Hongyan Chemical Reagent; AR 99.5%), manganese acetate tetrahydrate (Mn(ac)$_2$•4H$_2$O; Damao Chemical Reagent; AR 99.0%), ferric chloride hexahydrate (FeCl$_3$·6H$_2$O; Kemiou Chemical Reagent; AR 99.0%),ethanol absolute (CH$_3$CH$_2$OH; Guanghua Chemical Reagent; AR 99.7%),ammonia solution (NH$_3$•H$_2$O;Guanghua Chemical Reagent; AR 25-28%), carbon paper were used as received unless stated otherwise. Doubly distilled water was used throughout the experiment.

2. Instrumentation

X-ray photoelectron spectroscopy (XPS) was carried out using a Kratos Axis Supra spectrometer at room temperature and ultra-high vacuum (UHV) conditions. The instrument was equipped with monochromatic Al Kα source 1486.6 eV (15 mA, 15 kV), and hemispherical analyser with hybrid magnetic and electrostatic lens for enhanced electron collection. Survey and detailed XPS spectra were acquired at normal emission with the fixed pass energy of 160 eV and 40 eV, respectively. All spectra were charge-corrected to the hydrocarbon peak set to 284.6 eV. The Kratos charge neutralizer system was used on all specimens. Data analysis was based on a standard deconvolution method using mixed Gaussian (G) and Lorentzian (L) line shape (G = 70% and L = 30%, Gaussian–Lorentzian product) for each component. Spectra were analyzed using CasaXPS software (version 2.3.16). X-ray diffraction (XRD) was acquired using (D8 ADV ANCE, Bruker) diffractometer having Cu Kα (λ=1.54 Å) source. The instrument was operated at 30 mA current voltage and 40 kV. Field emission scanning electron microscope (S-4800, Hitachi, Japan) and transmission electron microscope (FEI-Tecnai G2 F20) were used to observe the morphology of the catalyst. ICP-AES parameters are the following: forward power 1350 W, plasma gas flow rate 12.0 L min^{-1}, nebulizer gas flow rate 1.0 L min^{-1}, auxiliary gas flow rate 1.0 L min^{-1}, sample uptake speed 50 rpm with white/orange Tygon tubing. A concentric nebulizer was used with a cyclonic spray chamber. No internal standard correction was applied for ICP-AES analysis.

3. X-ray photoelectron spectroscopy
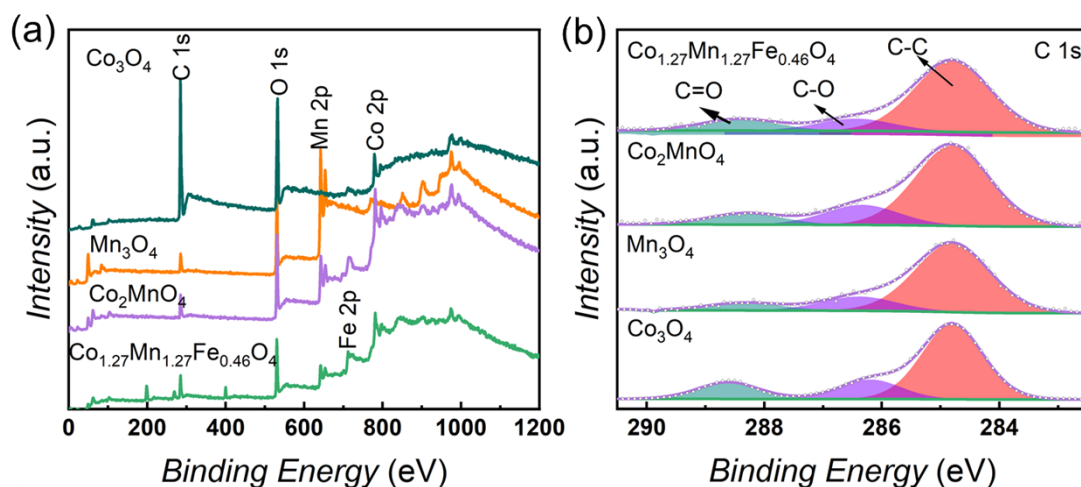
Figure S1. (a) XPS survey spectra of the Co_3O_4, Mn_3O_4, Co_2MnO_4 and $Co_{1.27}Mn_{1.27}Fe_{0.46}O_4$/CP; (b) Deconvoluted high-resolution XPS spectra of the C 1s region of Co_3O_4, Mn_3O_4, Co_2MnO_4 and $Co_{1.27}Mn_{1.27}Fe_{0.46}O_4$/CP.
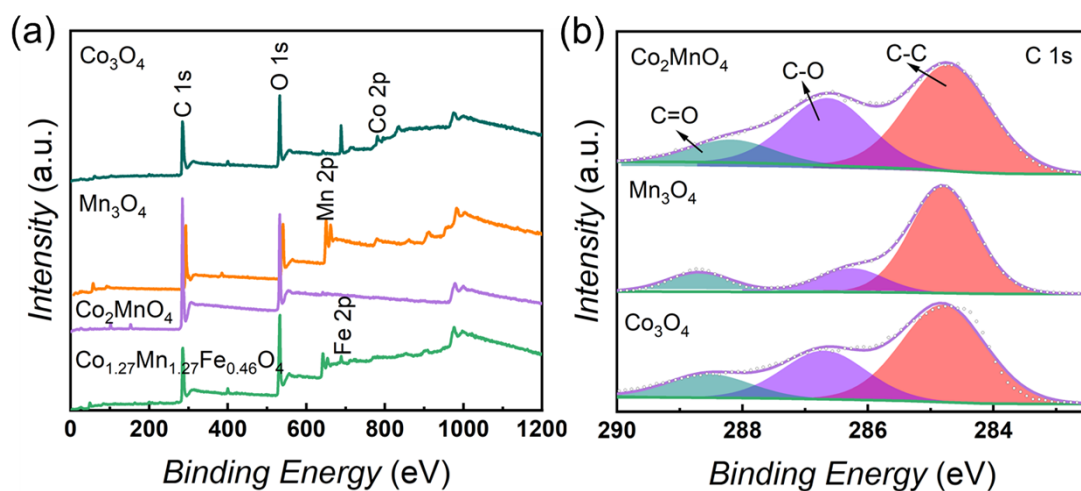
Figure S2. (a) XPS survey spectra of the Co_3O_4, Mn_3O_4, Co_2MnO_4 and $Co_{1.27}Mn_{1.27}Fe_{0.46}O_4$/CP after the long-term galvanostatic test; (b) Deconvoluted high-resolution XPS spectra of the C 1s region of Co_3O_4, Mn_3O_4, Co_2MnO_4 and $Co_{1.27}Mn_{1.27}Fe_{0.46}O_4$/CP after the long-term galvanostatic test.

4. X-ray diffraction
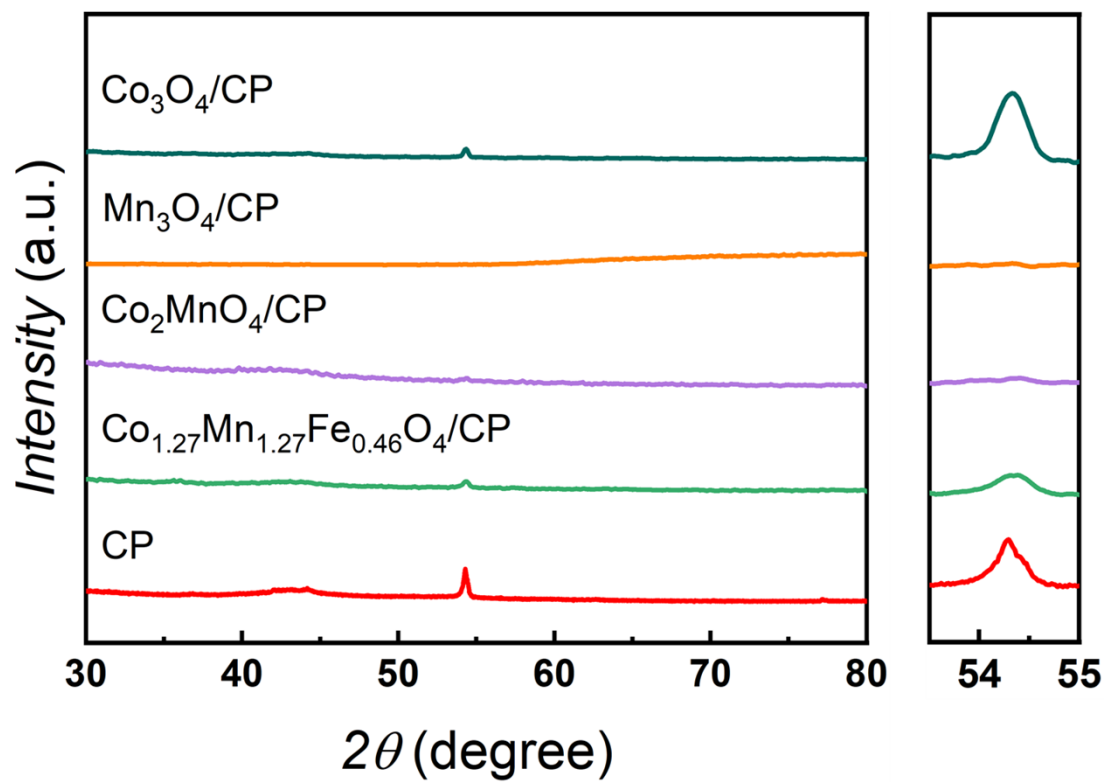
Figure S3. XRD patterns of the Co_3O_4, Mn_3O_4, Co_2MnO_4, $Co_{1.27}Mn_{1.27}Fe_{0.46}O_4$/CP and carbon paper after long-term galvanostatic test.

5. EDS and ICP-AES

Table S1. Contents of the spinel-type oxides

		Atomic Percentage (%)			
		Co	Mn	Fe	O
Co_3O_4	EDS	39.56	-	-	60.44
Mn_3O_4	EDS	38.43	-	-	61.57
Co_2MnO_4	EDS	21.74	17.38	-	60.88
$Co_{1.27}Mn_{1.27}Fe_{0.46}O_4$	ICP-AES	41.74	42.93	15.34	-
	EDS	16.39	15.31	7.89	60.41

Table S2. The amounts of elements dissolved into the electrolytes after long-term

OER

ICP-AES		Co	Mn	Fe
Dissolved mass (mg)	Co_3O_4	0.692	-	-
	Mn_3O_4	-	0.690	-
	Co_2MnO_4	1.022	0.595	-
	$Co_{1.27}Mn_{1.27}Fe_{0.46}O_4$	0.401	0.213	0.058
Atomic Percentage(%)	Co_3O_4	17.31	-	-
	Mn_3O_4	-	17.24	-
	Co_2MnO_4	20.88	13.70	-

	Co$_{1.27}$Mn$_{1.27}$Fe$_{0.46}$O$_4$	10.04	5.34	1.45

Table S3. The content of different oxygen groups

XPS		Atomic Percentage (%)		
		-O	-OH	-H$_2$O
Before	Co$_3$O$_4$	12.24	45.06	42.69
	Mn$_3$O$_4$	74.64	18.97	6.39
	Co$_2$MnO$_4$	67.05	23.75	9.20
	Co$_{1.27}$Mn$_{1.27}$Fe$_{0.46}$O$_4$	62.10	31.01	6.90
After	Co$_3$O$_4$	13.81	75.78	10.41
	Mn$_3$O$_4$	25.85	41.81	32.34
	Co$_2$MnO$_4$	12.62	72.66	14.72
	Co$_{1.27}$Mn$_{1.27}$Fe$_{0.46}$O$_4$	19.51	38.76	41.73

6. Electrochemistry
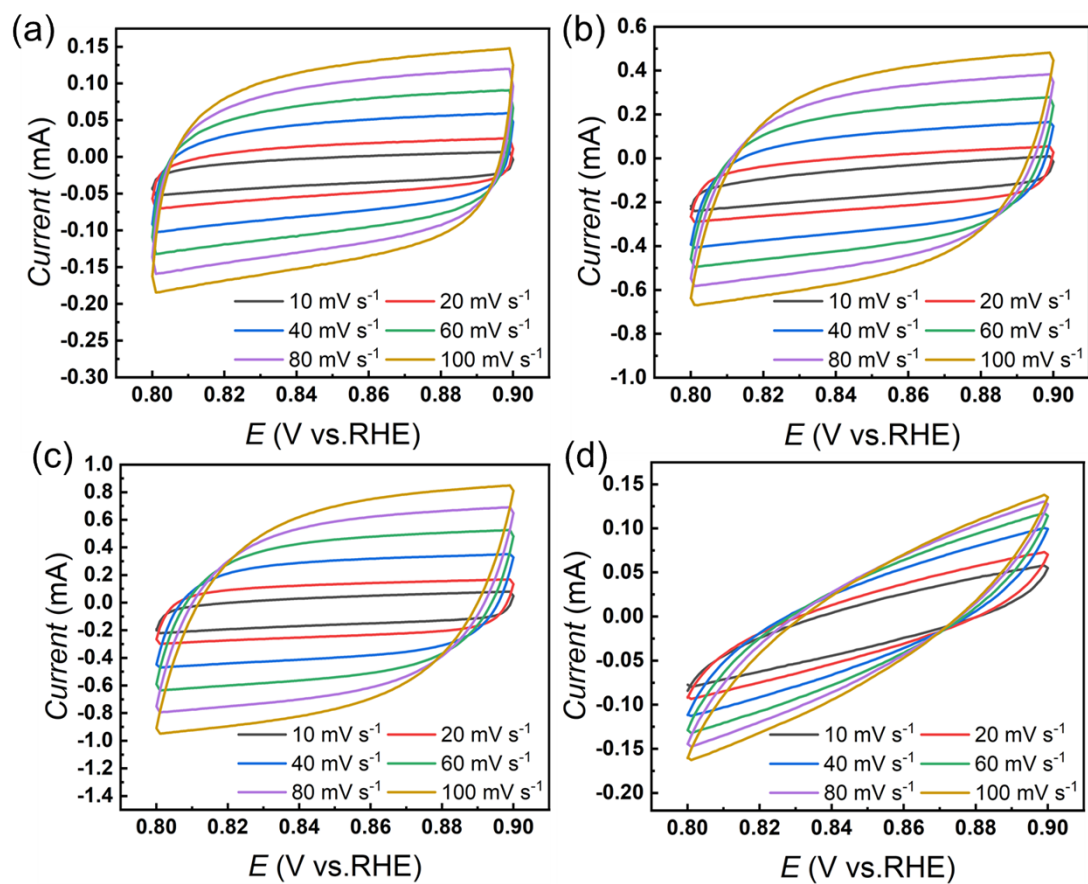
Figure S4. (a-d) CV of Co_3O_4, Mn_3O_4, Co_2MnO_4 and $Co_{1.27}Mn_{1.27}Fe_{0.46}O_4$/CP at different scan rates (10, 20, 40, 60, 80, and 100 mV s^{-1}) in 0.8 - 0.9 V in 1 M $HClO_4$.

Theoretically, a simple electrochemical redox reaction can be described by the Butler-Volmer equation:

$$j = j_0\{\exp(-\alpha f\eta) - \exp[(1-\alpha)f\eta]\} \qquad (1)$$

By taking logarithm of Eq. 1, and assuming the reverse reaction negligible, there is

$$\log j = \log j_0 + \alpha f\eta/2.303RT \qquad (2)$$

where α is the transfer coefficient, f denotes F/RT (F: the Faraday's constant, R: the universal gas constant, T: the absolute temperature), and j_0 is the exchange current density. Therefore, by plotting the $\log j$ vs. η plot, the j_0 can be acquired from the intercept.

The j_0 of MOR for Co_3O_4, Mn_3O_4, Co_2MnO_4 and $Co_{1.27}Mn_{1.27}Fe_{0.46}O_4/CP$ are 2.45×10^{-5} mA cm^{-2}, 2.51×10^{-4} mA cm^{-2}, 1.62×10^{-6} mA cm^{-2} and 4.58×10^{-8} mA cm^{-2}, respectively.
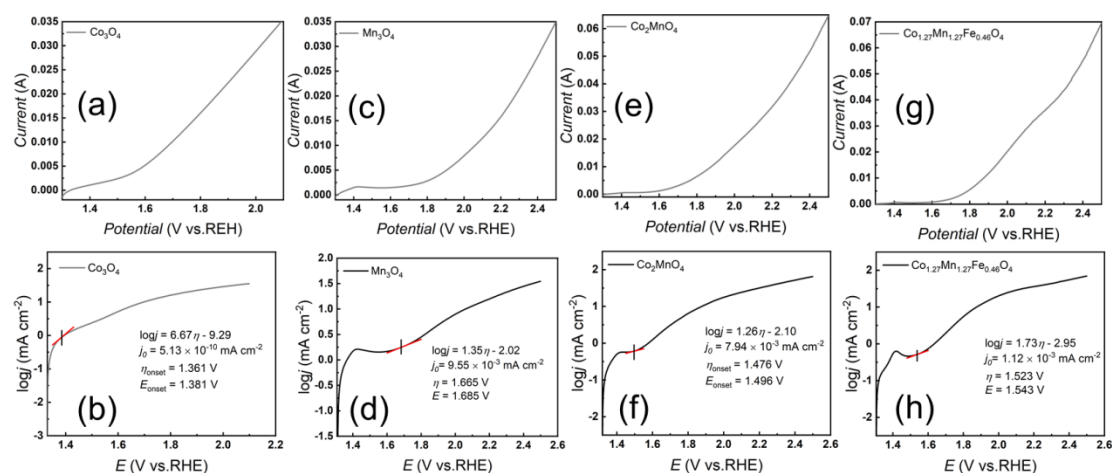
Figure S5. The LSV of the Co_3O_4, Mn_3O_4, Co_2MnO_4 and $Co_{1.27}Mn_{1.27}Fe_{0.46}O_4/CP$ electrodes in 0.5 M CH3OH + 1 M HClO$_4$ (scan rate 5 mV s^{-1}).

Table S4. EIS fitting results

|	R_S/Ω	Error/%	R_{CT}/Ω	Error/%
Co_3O_4	10.73	0.172	9.63	1.346
Mn_3O_4	17.60	0.493	218.90	3.754
Co_2MnO_4	16.54	0.578	60.51	2.539
$Co_{1.27}Mn_{1.27}Fe_{0.46}O_4$	12.85	0.295	39.87	0.834
Co_3O_4 after galvanostatic OER test	11.34	0.404	10.72	1.698

7. Activity comparison

Table S5. OER activity comparison in acid

Catalysts	Electrolyte	η@10 mA cm^{-2}/mV	Tafel Slope/ mV dec^{-1}	Stability/h	References
Co_3O_4/CP	0.1 M $HClO_4$	336	74.7	28	This work
Co_3O_4@C/CP	0.5 M H_2SO_4	370	82	86.8	[1]
Co_3O_4/CeO_2/FTO	0.5 M H_2SO_4	423	88.1	>50 h	[2]
Ag-Co_3O_4	0.5 M H_2SO_4	680	219	12	[3]
Ir-Co_3O_4	0.5 M H_2SO_4	225	64.1	130	[4]
P-Co_3O_4	0.1 M $HClO_4$	400	98	30	[5]
Co_3S_4@rGO	0.5 M H_2SO_4	350	65	>8	[6]
$RuO_2(Co,Mn)_3O_4$/ CC	0.5 M H_2SO_4	270	77	24	[7]
HNC-Co	0.5 M H_2SO_4	265	85	-	[8]
AlNiCoIrMo	0.5 M H_2SO_4	233	55.2	-	[9]

8. TEM
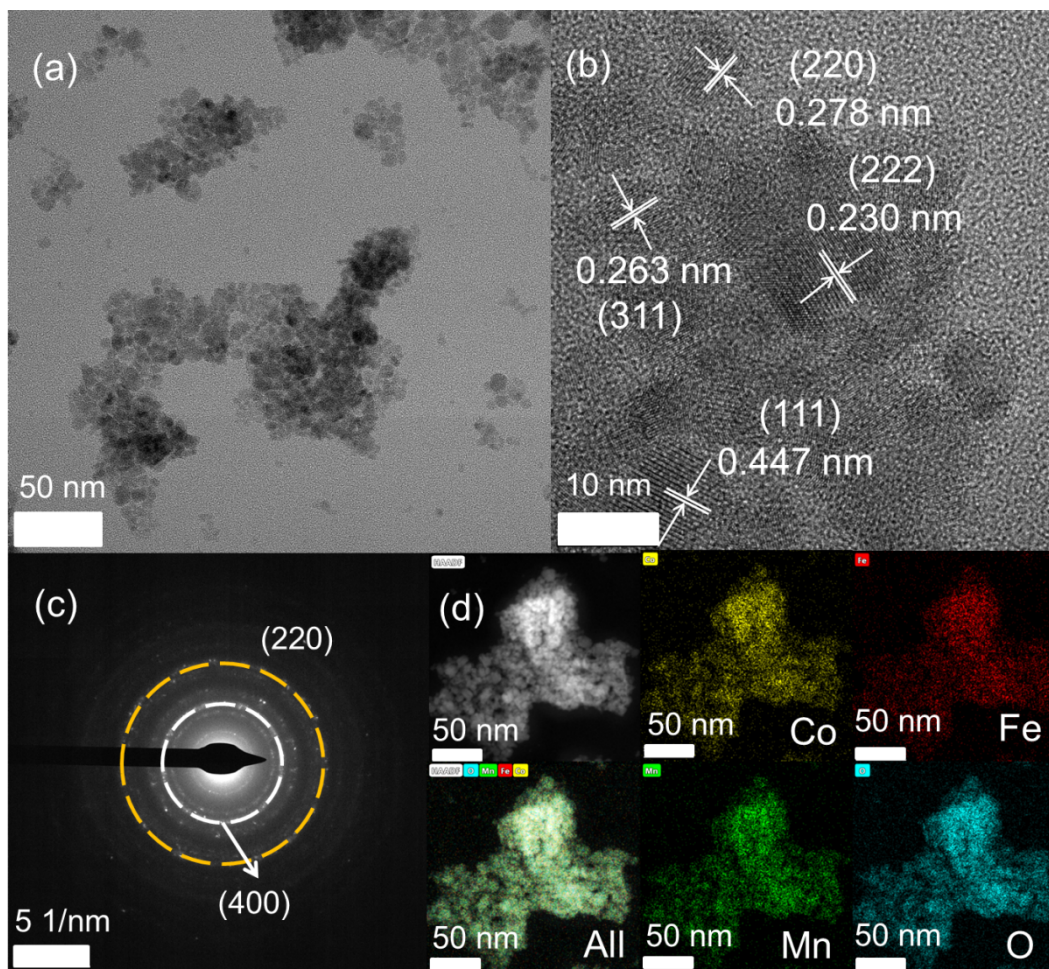
Figure S6. (a) TEM image of the $Co_{1.27}Mn_{1.27}Fe_{0.46}O_4$; (b) High resolution TEM image of the $Co_{1.27}Mn_{1.27}Fe_{0.46}O_4$; (c) SAED pattern of the $Co_{1.27}Mn_{1.27}Fe_{0.46}O_4$; (d) Elemental mapping and HAADF image of the $Co_{1.27}Mn_{1.27}Fe_{0.46}O_4$.

9. References

[1]   YANG X, LI H, LU A-Y, et al. Highly acid-durable carbon coated Co_3O_4 nanoarrays as efficient oxygen evolution electrocatalysts [J]. Nano Energy, 2016, 25: 42-50.

[2]   HUANG J, SHENG H, ROSS R D, et al. Modifying redox properties and local bonding of Co_3O_4 by CeO_2 enhances oxygen evolution catalysis in acid [J]. Nature communications, 2021, 12(1): 3036.

[3]   YAN K-L, CHI J-Q, XIE J-Y, et al. Mesoporous Ag-doped Co_3O_4 nanowire arrays supported on FTO as efficient electrocatalysts for oxygen evolution reaction in acidic media [J]. Renewable Energy, 2018, 119: 54-61.

[4]   XIE Y, SU Y, QIN H, et al. Ir-doped Co_3O_4 as efficient electrocatalyst for acidic oxygen evolution reaction [J]. International Journal of Hydrogen Energy, 2023.

[5]   SHANG F, HE H, LI P, et al. PO6 geometric configuration unit enhanced electrocatalytic performance of Co_3O_4 in acidic oxygen evolution [J]. Journal of colloid and interface science, 2023, 641: 329-37.

[6]   KUMAR R S, KARTHIKEYAN S, RAMAKRISHNAN S, et al. Anion dependency of spinel type cobalt catalysts for efficient overall water splitting in an acid medium [J]. Chemical Engineering Journal, 2023, 451: 138471.

[7]   NIU S, KONG X-P, LI S, et al. Low Ru loading $RuO_2/(Co, Mn)_3O_4$ nanocomposite with modulated electronic structure for efficient oxygen evolution reaction in acid [J]. Applied Catalysis B: Environmental, 2021, 297: 120442.

[8]   SU H, ZHAO X, CHENG W, et al. Hetero-N-coordinated Co single sites with high turnover frequency for efficient electrocatalytic oxygen evolution in an acidic medium [J]. ACS Energy Letters, 2019, 4(8): 1816-22.

[9]   JIN Z, LV J, JIA H, et al. Nanoporous Al-Ni-Co-Ir-Mo high-entropy alloy for record-high water splitting activity in acidic environments [J]. Small, 2019, 15(47): 1904180.